Extreme Mechanics Letters 70 (2024) 102186

Contents lists available at ScienceDirect

Extreme Mechanics Letters

journal homepage: www.elsevier.com/locate/eml

# Current density alters the mechanical stresses during electrodeposition of lithium metal anodes

Jungho Shin , Matt Pharr [*,1]

*Department of Mechanical Engineering, Texas A&M University, College Station, TX 77845-3255, USA*

ARTICLE INFO

*Keywords:*
Lithium metal
Batteries
Mechanics
Electrochemistry
Electro-chemo-mechanics
Current density

ABSTRACT

"Lithium metal" batteries operate via electroplating/stripping of Li metal and promise vast theoretical capacities. However, significant technical barriers must be addressed prior to commercialization. The primary challenges include the generation of mechanical stresses and strains due to "infinite volume expansion," as well as non-uniform deposition of lithium metal, which often leads to dendrite formation and growth. Lithium dendrite formation is particularly critical, as dendrites can penetrate solid-state electrolytes, eventually shorting to the cathode, thereby diminishing the capacity of the battery and inducing severe safety hazards. These primary issues are intrinsically linked to the mechanical behavior of lithium; as such, this study focuses on the mechanical response of lithium electrodeposition under various electrochemical conditions. Experimental tests herein reveal that larger applied current densities induce significantly larger mechanical stresses during electroplating of Li metal. This manuscript concludes by detailing practical implications of these experimental observations, particularly regarding dendrite growth through solid-state electrolytes of solid-state batteries.

## 1. Introduction

Advances in rechargeable battery technologies have brought about improvements in the performance of electronic devices. Current research efforts aim to push the advances further by studying various metal-based anodes for rechargeable batteries with significantly improved capacities beyond conventional graphite-based anodes (theoretically 350 mAh/g for graphite vs. 3860 mAh/g for Li, 4200 mAh/g for Si, 3832 mAh/g for Mg, etc.) [1–8]. Of the potential anode materials, lithium metal is a tantalizing choice in that it possesses the lowest electrochemical potential of −3.04 V (vs. standard potential), is the lowest density metal, and has a relatively high theoretical capacity [9–12]. However, developing practical and robust lithium metal anodes has been impeded by several challenges, including dendrite formation, non-uniform plating/stripping, and formation of "dead" regions [13–16]. To overcome these obstacles, it is imperative to understand both the electrochemical and mechanical behavior of lithium metal anodes during electrochemical cycling.

One of the key challenges in the development of lithium metal anodes is understanding its underlying mechanics [17,18]. Specifically, Li metal anodes undergo "infinite volume change" during electrochemical cycling due to its host-less nature (i.e., it involves plating/stripping during charge/discharge) [19,20]. Correspondingly, the electrochemical plating and stripping process may generate significant mechanical stresses in the anode [17,21]. For example, Cho et al. conducted in-situ stress measurements during plating of lithium metal anodes and observed that compressive stresses generated can induce surface wrinkling, which in turn can result in ratcheting and delamination of the surface layer [17]. This mechanical degradation readily deteriorates the electrochemical performance of a lithium metal battery, forming irregular morphology of the Li layer, a thick layer of SEI (Solid-Electrolyte Interphase), and/or electronically isolated Li, also known as "dead" Li [22–25]. Indeed, Chen et al. has reported that the amount of dead Li accumulates as electrochemical cycling continues in Li-Li symmetric cells, which leads to severe capacity fade of the cells [22].

Another challenge in lithium metal anodes is the formation of lithium dendrites, which can lead to short-circuits, induce failure of the entire battery system, and even increase the risk of fires and explosions [19,26,27]. Even when integrating with solid-state electrolytes, needle-like structures can originate from the Li anode and then penetrate through the solid-state electrolyte all the way to the cathode, thus causing electrical short-circuits [21,28,29]. While the mechanism of

* Corresponding author.
*E-mail addresses:* jungho.shin0912@tamu.edu (J. Shin), m-pharr@tamu.edu (M. Pharr).
[1] Present/Permanent address: Mechanical Engineering Office Building 221, 3123 TAMU, College Station, TX 77843–3123

https://doi.org/10.1016/j.eml.2024.102186
Received 9 April 2024; Received in revised form 19 June 2024; Accepted 21 June 2024
Available online 27 June 2024

penetration through the solid-state electrolyte is not yet fully understood, one proposed theory is that Li metal can fill in crack-like regions in the solid electrolyte, and in doing so, exert a pressure on the crack walls, which can further propagate the crack forward in the solid-state electrolyte [30,31]. This process occurs iteratively, thus forming a "dendritic" structure, and can eventually propagate all the way to the cathode, producing a short circuit in the battery. To prevent this lithium penetration, researchers have studied several strategies including enhancing the mechanical strength and fracture toughness of the solid-state electrolyte, as well as using additives to promote uniform lithium deposition [32,33]. For instance, Athanasiou et al. developed a solid-state electrolyte ($Li_{1+x}Al_xTi_{2-x}(PO_4)_3$) with high fracture toughness to resist lithium penetration by incorporating a 2D material (reduced graphene oxide) into the solid-state electrolyte [33]. Lee et al. developed a solid-state battery with a Ag-C nanocomposite layer as the anode, where Ag is soluble in lithium and reduces the nucleation energy of lithium, thereby enabling uniform lithium plating [34]. However, these studies have primarily concentrated on developing intricate fabrication and processing techniques to mitigate lithium penetration, rather than investigating the mechanical characteristics of lithium metal itself during electrochemical cycling.

To improve robustness during electrochemical cycling, a deeper understanding of the mechanical properties of lithium metal and its mechanical behavior during electrochemical cycling is needed. However, relatively little is known regarding the mechanical behaviors of Li due to its extreme reactivity in air [35–37]. Fincher et al. reported the yield strength of Li between 0.57 and 1.26 MPa for strain rates from $5\times10^{-4}$ to $5\times10^{-1}$ $s^{-1}$ under compression, and they observed significant "size effects" (length scale dependent hardness/strength) at small (100's of nm) length scales [36]. Masias et al. found that Li metal exhibited power law creep behavior over a wide range of strain rates, suggesting that its deformation mechanism is largely mediated by diffusion[37]. However, these studies did not examine the mechanical behavior of lithium metal anode during electrochemical cycling. By contrast, Cho et al. experimentally investigated in-situ stress evolution in Li metal anodes and observed a rapid increase and eventual saturation in compressive stress during electroplating [17]. They also developed an analytical model that suggested that compressive stresses generated in the surface layer can lead to surface wrinkling and strain in the underlying soft Li metal. However, they did not evaluate the mechanical behaviors of Li metal anodes under various electrochemical cycling conditions. Given that lithium metal exhibits extreme strain-rate sensitivity at room temperature and significant size effect at small scales, it may exhibit considerably different behaviors while electrochemically cycling under different conditions and at different length scales (e.g., of the electrodeposit). All in all, it is critical to understand the properties of lithium metal and the corresponding ramifications under various charging conditions to prevent potential mechanical degradation and safety issues in the future. To this end, in this manuscript we examine the mechanical behavior of the Li metal anode under various charging conditions to assess its sensitivity to varying current densities. We also performed nanoindentation creep tests on bulk Li and electroplated Li to compare their mechanical characteristics. Finally, bearing in mind that the electroplating and Li dendrite growth share some similar growth mechanisms, we further discuss the implications of the mechanics of Li metal anodes observed in the study in the context of dendrite growth.

## 2. Materials and methods

### 2.1. Electrode preparation

We utilized mirror-polished 304 stainless steel plates with a thickness of 450 μm from JW Metal Products as the current collector for the working electrodes. The plates were thoroughly washed with acetone and isopropanol and placed into an E-beam deposition chamber (Lesker PVD 75 Electron Beam Evaporation) with a base pressure of $5 \times 10^{-6}$ Torr. First, a thin layer (~10 nm) of titanium was deposited onto a stainless-steel plate at a deposition rate of 0.5 Å/s as an adhesion layer, followed by a 40 nm thick magnesium layer being deposited on top of the titanium layer at a deposition rate of 1.0 Å/s. We deposited a thin magnesium layer to promote uniform Li deposition during electrochemical cycling. After E-beam deposition, we transferred the samples to an Ar-filled glovebox using a hermetic vacuum transfer vessel (VWR® Desi-Vac™ Container) which engendered less than 30 seconds of total air-exposure during the transfer process. The glovebox was maintained with $O_2$ and moisture ($H_2O$) levels less than 1.0 ppm each.

### 2.2. Cell preparation

A customized spilt cell with a quartz window (MTI Corporation) was used for electrochemical measurements. The cell was assembled in an Ar-filled glovebox (with $O_2$ and moisture ($H_2O$) levels less than 1.0 ppm each) and consisted of the Mg-deposited stainless plate as the working electrode, a Celgard 2400 separator (MTI Inc.), a Li ribbon (Sigma Aldrich, Product No. 265985) as the counter electrode, and 1.0 M $LiPF_6$ in EC/DMC (ethyl carbonate/dimethyl carbonate, MTI Inc.) as the electrolyte. The mirror-polished surface (i.e., the "back side") of the stainless steel was positioned just below the transparent quartz window. The specific cell configuration used can be found in Supplementary Information Figure S1. After assembly, the cell was allowed to rest for 5 hours prior to applying current to the cell.

### 2.3. Pre-lithiation and pre-plating

First, the cell was galvanostatically discharged at a relatively low current density of 5 μA/$cm^2$ to fully lithiate the Mg layer (herein, referred to as "pre-lithiation"), which alloyed the Mg with Li, likely forming a Li-rich β-LiMg alloy phase. Following this process, the cell was discharged at a relatively higher current density of 120 μA/$cm^2$ (herein, referred to as "pre-plating"), which electrodeposited a relatively thicker layer of lithium onto the surface of the lithiated magnesium layer. We adopted and modified the method presented by Cho et al. [17]. Namely, similarities exist between our study and theirs in evaluating the stress caused by the deposition of a new lithium layer following an initial "pre-plating" of lithium. However, in terms of estimating mechanical stress, they utilized force and moment equilibrium equations, whereas we implemented Stoney's equation for our estimations. A detailed description of these steps are described in Supplementary Information Note S1 and Note S2.

### 2.4. Galvanostatic discharging & current density jump testing

After preparation (pre-lithiation and pre-plating), specimens were discharged at three different current densities of 40 μA/$cm^2$, 150 μA/$cm^2$, and 350 μA/$cm^2$. All samples were discharged up to the same nominal capacity of 1500 μAh. For the current density jump testing, the cell was first held under open-circuit conditions for two hours, followed by discharging at four different current densities of 40 μA/$cm^2$, 150 μA/$cm^2$, 350 μA/$cm^2$, and 600 μA/$cm^2$ with a two-hour open-circuit segment between each current density. All experiments were conducted at room temperature (~25 °C).

### 2.5. In-situ mechanical measurements

A multibeam optical stress sensor (MOS, k-Space Associates) was used to measure the changes in curvature of the anode/substrate during electrochemical testing. The laser array (2 × 2 or 3 × 3) from the laser source was reflected off the mirror-polished stainless-steel current collector, and a CCD laser detector continuously monitored the distance between each laser spot. By monitoring the relative change in spot spacing, we could obtain the curvature change (ΔK) of the substrate during electrochemical cycling:

$$\Delta K = \frac{d_0 - d}{d_0} \left[\frac{\cos\alpha}{2L}\right]$$

where $d$ is distance between two adjacent laser spots at a given time, $d_0$ is initial distance between the laser spots, $\alpha$ is the reflection angle of the laser beams, and $L$ is the distance between the electrochemical cell and the CCD camera [38]. Using the measured curvature, the average stress changes ($\Delta\sigma_{Li}$) induced by Li plating was estimated through Stoney's equation, and detailed calculations are described in Supplementary Information Note S2.

### 2.6. Nanoindentation

For the nanoindentation tests, we prepared two distinct types of lithium samples: a) bulk lithium (lithium ribbon) and b) electroplated lithium. We carefully scraped the surface of the lithium ribbon inside the Ar-filled glovebox to remove any surface contaminants, followed by pressing it in a crimping machine to smooth out its surface roughness. As for the electroplated Li, it was thoroughly washed with anhydrous dimethoxyethane (DME) and subsequently dried in an Ar-filled glovebox. Afterwards, each sample was securely adhered to the nanoindentation sample puck using Crystalbond Adhesive (Ted Pella, 821–1), and the nanoindentation tests were performed with a Berkovich indenter in the continuous stiffness measurement (CSM) mode [39]. All tests were carried out under mineral oil to avoid any undesirable chemical reactions with air. To evaluate the appropriateness of using mineral oil, we conducted a comparative analysis between nanoindentation test data of bulk lithium performed in an Ar-filled glovebox and the data utilized herein conducted outside the glovebox but under mineral oil [36]. The differences were found to be negligible, indicating that the use of mineral oil did not significantly alter the nanoindentation data. Tests were carried out at a nominal constant strain rate (loading rate by load) of 0.05 $s^{-1}$ up to a displacement of 1 μm, at which point the corresponding load was held for 1 minute prior to unloading. After nanoindentation testing, there were no noticeable color changes visible (i.e., as potentially arising from chemical reactions with air) due to the presence of the protective layer of mineral oil.

### 2.7. Structural and morphological characterization

The electrochemical cell was disassembled in an Ar-filled glovebox after electroplating and the surface was rinsed with anhydrous DME prior to examination. For X-ray Diffraction (XRD, BRUKER D8 X-ray) Vaseline petroleum jelly was applied to the top of the electrode to protect the sample surface from undesirable chemical reactions with air during the measurement. XRD patterns were measured at the range of 30° - 60° with a Cu Kα source. For the scanning electron microscope studies (SEM, FEI Quanta 600) the sample was transferred via a hermetic vacuum transfer vessel and placed onto the SEM stage. We estimate that the air-exposure time was less than 30 seconds during this process.

## 3. Results and discussions

This work aims to characterize mechanical stresses generated during electrodeposition of lithium metal under different electrochemical loading conditions (charging/deposition rates). Electrochemical deposition of Li often leads to uneven and irregular structures forming on the electrode, producing undesirable structures that are often termed "lithium dendrites"[28,40,41]. The exact reasons for the nonuniform Li deposition are not clearly understood, but the reported factors include uneven current distribution across the surface and instability of the electrolyte [42,43]. For the purposes of our study, it is critical to achieve fairly uniform deposition of Li for accurate and meaningful measurements of the average stress across the surface of the anode during lithium plating. Wang et al. reported an increase in the wettability of Li on a surface upon adding elements such as indium, tin, and magnesium [44,45]. With this study in mind, herein we deposited a relatively thin magnesium layer of 40 nm on a stainless-steel current collector prior to the lithium deposition, as to promote more spatially uniform deposition of Li. Prior to mechanical stress measurements, the Mg layer was galvanostatically pre-lithiated at a relatively low current density of 5 μA/$cm^2$, to de-convolute any effects caused by the volume expansion of Mg upon lithiation (herein, referred to as "pre-lithiation"). Afterwards, a relatively thick lithium layer, approximately 10 μm in thickness, was deposited on the lithiated Mg layer (herein, referred to as "pre-plating"). This layer reduces the relative roughness of the Li (roughness/total thickness of the lithium layer), thus enhancing the accuracy of mechanical stress measurements. Supplementary Information Note S1 details the electrochemical loading sequences utilized in this study.

Simultaneous to the electrodeposition of Li, the changes in curvature of the anode (and substrate) were measured using a multibeam optical stress sensor (MOS system), as shown in Fig. 1. In our sign convention, a negative curvature indicates that compressive stress is being generated in the lithiated layers. Supplementary Information Note S1 shows that the sample preparation process (pre-lithiation and pre-plating) produced a compressive residual stress in the electrode prior to our reported stress measurements (i.e., prior to those shown in Figs. 3 and 4). The residual stress estimation is detailed in Supplementary Information Note S3.

Fig. 2 and Figure S2 show SEM images of an electrodeposit of lithium and confirm that a relatively uniform Li layer was achieved through our fabrication and electrodeposition processes, largely owing to the presence of the lithiophilic Mg underlayer. In Fig. 2b, the surface was ion-milled and tilted in the view by a 30-degree angle, providing a detailed cross-sectional SEM image of the Li layer. Within the lithium layer, numerous voids were detected, which is a typical characteristic of electrochemical lithium deposition [46–48]. Indeed, Kanamori et al. observed that Li electrodeposition, in the absence of applied pressure, resulted in dendritic (porous) lithium structures on copper substrate [46]. Likewise, Guo et al. reported the electrodeposition of a porous Li layer on Cu and Co/$Co_4$N-NC (hollow nitrogen-doped carbon nanocubes) electrodes [47]. Herein, the MOS system measures the overall average stress across the entire surface, rather than measuring localized stresses in specific (small) regions (e.g., near voids). Consequently, the stresses reported herein will likely underestimate the stresses that would be generated if fully dense electrodeposition could be achieved. Furthermore, Figure S3 displays XRD patterns of the electrochemically deposited lithium layer, with an ICSD database of pure lithium for comparison. We note that there is a slight presence of lithium oxide, likely formed during the transfer process into the SEM (which involved approximately 30 seconds of air exposure during the process).

The curvature ($K = \frac{1}{r}$, where r is the radius of the anode/substrate) of the anode was monitored during electrodeposition using MOS system, and the average stress induced by Li plating was estimated using Stoney's equation [49]:

$$\Delta\sigma_{Li} = \frac{E_c h_c^{\,2}}{6h_f(1-\nu_c)} \Delta K$$

where $E_c$ is the elastic modulus of the stainless-steel current collector, $h_c$ is the thickness of the stainless-steel current collector, $\nu_c$ is Poisson's ratio of the stainless-steel current collector, and $h_f$ is the thickness of Li layer. Detailed assumptions and calculations can be found in Supplementary Information Note S2. Here, we are reporting/estimating the 'in-plane true stress' by assuming that $h_f$ varies in accordance with the linear change in thickness due to time from Li deposition (i.e., by relating to the electrochemical loading conditions, as described in Supplementary Information Note S2). Additionally, it is important to note that the thickness estimation assumes a completely dense Li layer, while the cross-sectional SEM image in Fig. 2 reveals the presence of numerous voids in the deposited Li layer, which may lead to underestimation of the actual layer thickness. With this issue in mind, we

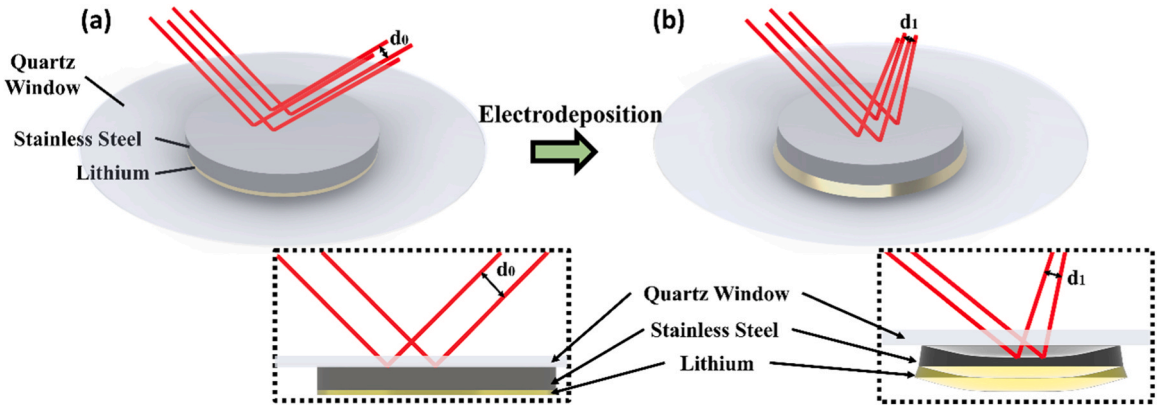


**Fig. 1.** Schematics of the experimental setup for mechanical stress measurements using a multibeam optical stress sensor (MOS) system. The specific cell configuration used for the in-situ mechanical measurement can be found in Supplementary Information Fig. S1.

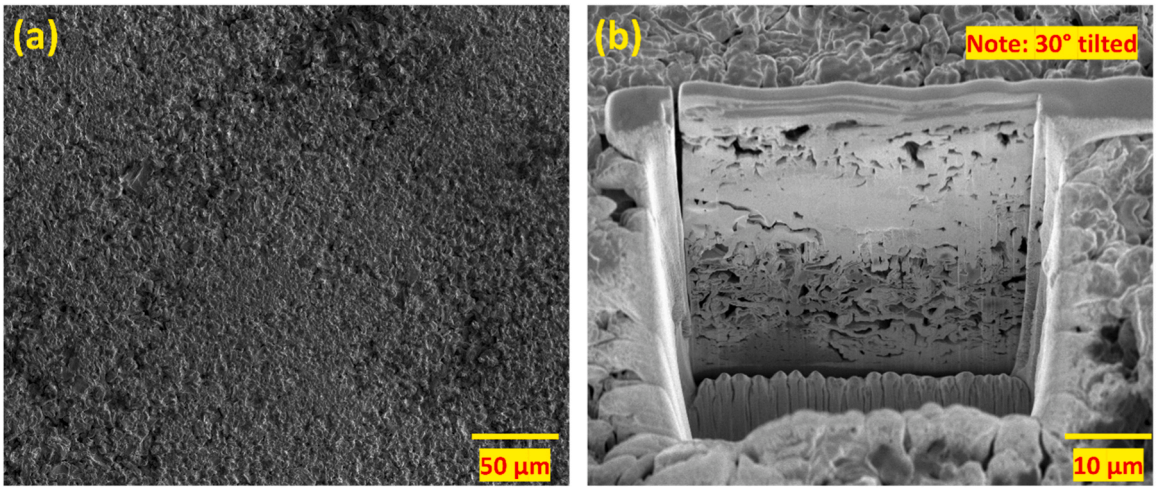


**Fig. 2.** Scanning electron microscopic (SEM) images of a (a) top view and (b) cross-sectional view of an electroplated Li layer. Zoomed-in images of the top surface at different levels of magnifications are available in Supplementary Information Fig. S2.

present both the stress changes calculated using Stoney's equation in the main manuscript (Fig. 3) and raw curvature changes, which exclude the effect of the thickness of the Li layer, in the Supplementary Information (Figure S4).

Fig. 3 shows the potential and corresponding stress measurements during galvanostatic plating of a Li metal anode under three different current densities of 40, 150, and 350 μA/cm$^2$. At the beginning of the discharging segment, the significant drop (in Fig. 3a-c) in potential may be attributable to a resistive interphase between the electrode, as well as the electrolyte and surface roughness of Li layer [26]. Additionally, if we define the overpotential as the potential necessary for electrodeposition relative to the equilibrium potential (here relative to 0 V vs. Li/Li$^+$), we note that the overpotential increases with higher applied currents. Namely, at 1500 μAh these potentials are −7 mV for 40 μA/cm$^2$, −13 mV for 150 μA/cm$^2$, and −26 mV for 350 μA/cm$^2$, respectively. This phenomenon arises from ohmic resistance causing a greater potential drop as the current increases [26]. The measured mechanical stresses (in Fig. 3d-f) arise from various atomistic and microstructural phenomena during electrodeposition, i.e., they indicate the total 'growth stress' of Li electrodeposition. Herein, the initial stress value begins from ∼ −120 kPa rather than 0 kPa due to the residual stress ($\sigma_r$) that results from sample conditioning ("pre-lithiation" and "pre-plating"), as discussed in Supplementary Information Note S3. Despite each Li metal anode in Fig. 3d-f being discharged to an identical capacity of 1500 μAh, we found that higher current densities induce higher levels of compressive stress. This critical insight demonstrates that the mechanical behavior of Li electrodeposition depends relatively strongly on the current density. Additionally, as previously mentioned, the voids within the lithium layer can lead to an underestimation of thickness, potentially resulting in an overestimation of stress change. As such, we also present raw curvature changes at various current densities, which exclude the effect of thickness estimation, in Figure S4. The normalization of time was based on the time required for each experiment to reach a capacity of 1500 μAh. These results still indicate that higher current densities result in more significant curvature changes (*i.e.*, forces generated / exerted on the substrate) at a given state of charge (*i.e.*, per each lithium atom deposited), which supports the main argument of this manuscript.

We also conducted 'current density-jump tests' in which a single electrochemical cell was subjected to galvanostatic discharging at various current densities of 40 μA/cm$^2$, 150 μA/cm$^2$, 350 μA/cm$^2$, and 600 μA/cm$^2$ for 2 hours each, with a 2-hour rest period (open-circuited) between each transition in current density. Fig. 4 shows the results of this study, which further attests to our observation that the mechanical behavior of Li electrodeposition strongly depends on the current density. Again, we observe that increasing the current density monotonically induced an increase in mechanical stress, which may have important ramifications in practical operation of Li-metal-based rechargeable batteries. Specifically, the changes in compressive stress during the deposition of 0.1 μm of Li metal were measured as 12.5 kPa/μm, 23.7 kPa/μm, 29.6 kPa/μm, and 16.3 kPa/μm, at current densities of 40 μA/

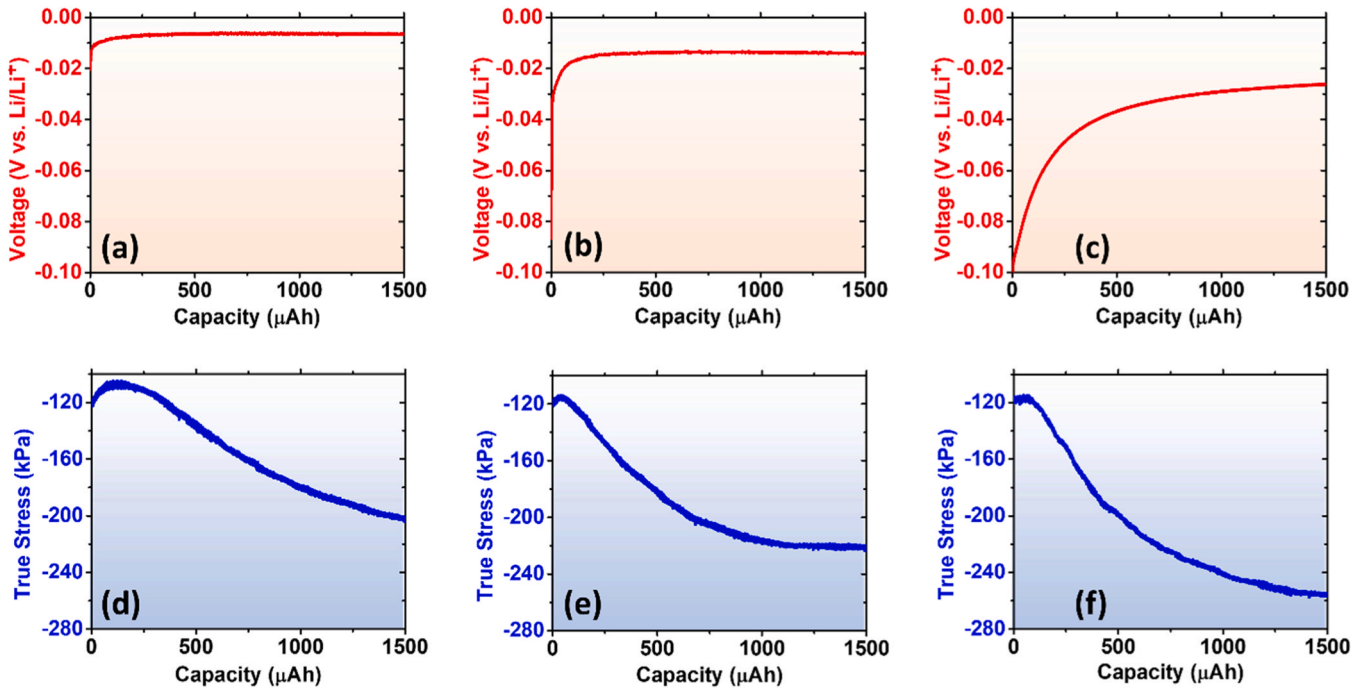


**Fig. 3.** (a)-(c) Voltage (V vs. $Li/Li^+$) and (d)-(f) corresponding true stress response at different current densities of (a), (d) 40 $\mu A/cm^2$, (b), (e) 150 $\mu A/cm^2$, and (c), (f) 350 $\mu A/cm^2$.

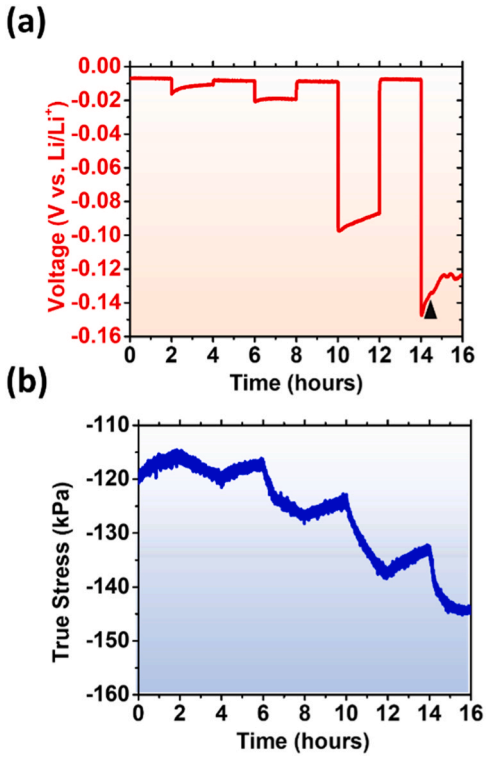


**Fig. 4.** (a) Voltage (V vs. $Li/Li^+$) and (b) corresponding true stress response of 'current density jump tests'. Prior to testing, "sample conditioning" ("pre-lithiation" and "pre-plating") was conducted. A Li metal anode was discharged at four distinct current densities of 40, 150, 350, and 600 $\mu A/cm^2$ during the respective time intervals of 2–4, 6–8, 10–12, and 14–16 hours. A 2-hour open-circuit period precedes each applied current density. The black triangle in (a) suggests a point in time at which unstable Li deposition (e.g., surface roughening, massive void nucleation) may have been induced, as based on the unstable voltage response.

$cm^2$, 150 $\mu A/cm^2$, 350 $\mu A/cm^2$, and 600 $\mu A/cm^2$, respectively. The reduced changes in stress and corresponding voltage fluctuations observed at 600 $\mu A/cm^2$ (Fig. 4) may suggest that the relatively high current density resulted in degradation, e.g., by producing a short circuit, more unstable deposition, etc., thereby resulting in (artificial) limited stress generation. Furthermore, the compressive stress continuously increases throughout the two-hour current application segments. Cho et al. reported that the compressive stress induced by the electrodeposition of Li increases and then becomes saturated [17]. In our studies, the two-hour segments of applying current seem insufficient for the stress to reach saturation. However, in Fig. 3, it was observed that the compressive indeed saturates. Additionally, at higher current densities, this saturation occurs at smaller capacities.

Previous studies have similarly identified rate-sensitive properties of lithium metal. For instance, Fincher et al. conducted uniaxial compression tests on pure lithium and discovered that its mechanical properties are highly sensitive to the applied strain-rate [36]. Masias et al. reported time-dependent mechanical properties of polycrystalline Li under tension and compression at room temperature [37]. Moreover, Ding et al. conducted research on the compressive creep deformation of lithium foil, revealing that the creep rates vary based on factors such as the geometry of the lithium specimen, the applied pressure, and the temperature [50]. Noting that increasing the current density during electrodeposition correspondingly increases the change in volume of the lithium deposit per time, one can conceivably draw connections between current density and strain rate (or creep rate), given their common conceptual thread of a change in dimension per time. As such, the rate-dependent electrodeposition behavior of lithium might be understood by examining the rate-dependent mechanical properties of lithium metal itself. For example, lithium metal's diffusion-mediated deformation mechanisms are likely to be a predominant factor in this process. Lithium exhibits relatively fast diffusion at room temperature due to its relatively low homologous temperature [36,51]; thus, deformation mechanisms involving diffusion are likely at play during normal operating conditions of lithium-based systems. As such, when applying lower current densities, lithium has more time to diffuse and facilitate diffusional-based deformation/growth mechanisms at relatively low

stresses. Conversely, when applying higher current densities, larger stresses may be built up (less time for lithium to diffuse to relax stresses) and/or other deformation mechanisms may dominate the deformation/growth process. Overall, we surmise that one key mechanism that governs rate-dependent stresses during electrodeposition of lithium is diffusion-mediated deformation of lithium. Still, we note that this idea is merely a hypothesis and corroboration of this hypothesis will require further detailed microstructural studies. However, it is imperative to note that strain-rate and current density are not connected here in a direct one-to-one sense. Notably, during electrodeposition, plating of lithium results in an increase in mass, while during mechanical testing, the mass of the metal remains unchanged. Likewise, plating of lithium involves distinct mechanisms of growth (e.g., related to details of nucleation, growth, crystallization, instabilities, epitaxy, columnar growth, island formation, coalescence, etc.), whereas pure mechanical loading involves the deformation mechanisms intrinsic to lithium (e.g., dislocation-mediated plastic flow, diffusion-mediated plastic flow, dislocation climb, etc.). As such, in-depth microstructural studies and theoretical analyses would be required to provide a comprehensive understanding of the mechanics of Li plating and/or to connect atomic/microstructural mechanisms of electrodeposition to mechanical deformation mechanisms of Li, which is beyond the scope of this study. Still, we surmise that electrodeposition and mechanical deformation of lithium likely share common traits through their shared microstructural features.

Additionally in Fig. 4, we observed a marked decrease in compressive stress during each 2-hour open-circuit interval. Figure S5 provides a zoomed-in view of an open circuit interval, highlighting the associated reductions in stress. Cho et al. also observed 'stress relaxation' during open circuit segments during Li plating, attributing this phenomenon to two primary mechanisms: 1) the dissolution of plated lithium back into the electrolyte and 2) the reduction of stress due to lithium's plastic flow [17]. In thin film mechanics, reductions in film stress are often observed during interruptions in the deposition process [52–54]. Namely, after deposition there is often a time-dependent shift in the mechanical stress toward tension, which has been attributed to the surface of the thin film stabilizing into a static configuration [53,54]. Microstructural features of these time-dependent processes include grain boundary area reduction, texture evolution, and vacancy annihilation [54]. Likewise, Floro et al. deposited various materials of Ag, Al, Ti, Ge, and Si on Si (001) substrates, and observed time-dependent stress relaxation, notably within a minute, during thin film growth interrupts [54].

Herein, we propose similar hypotheses that our observed reduction in mechanical stress during open circuit conditions is most likely due to viscoplastic behavior of lithium metal itself. Indeed, Li metal exhibits power-law creep with very large stress exponents, meaning that (creep) strain rate is quite sensitive to the applied stress level [36]. Specifically, the stress levels induced herein by electrodeposition are relatively low (< 300 kPa), which likely leads to a relatively slow reduction in stress during open circuit conditions. Similarly, Cho et al. observed stress reduction in a Li metal anode over considerable timespans (>10 hours) during open circuit segments [17]. Another potential explanation of the reduction in stress during open-circuit conditions is that chemical side reactions occur, which can alter the state of stress in the electrodeposit. An example of a "side reaction" that could lead to our observed behavior is the dissolution of lithium metal back into the electrolyte. Indeed, relative recent research has observed lithium dissolving into the electrolyte during open circuit conditions [26,55]. These chemical reactions typically occur over extended timescales and evolve over time. All in all, drawing insights from previous studies, both mechanics, particularly creep-type deformation, and electrochemical side reactions represent potential contributors to our observed stress reduction during open circuit conditions.

Fig. 5 shows results of nanoindentation creep tests on both bulk (Fig. 5a) and electroplated lithium (Fig. 5b), as to compare their mechanical characteristics. We note that the nanoindentation experiment was conducted under mineral oil to help mitigate any undesirable chemical reactions with air. The tests involved gradually increasing the load until reaching a nanoindentation displacement of 1 μm, and then holding the load constant at the maximum load for one minute, thereby allowing us to examine the time dependent (creep-type) behavior of Li metal. In Fig. 5a, we observed an increase in displacement of about 243 nm (*on average*) during the one-minute hold segment at the maximum load, which is indicative of a significant time-dependent creep-type behavior of bulk Li foil. The electroplated lithium shown in Fig. 5b demonstrated a similar increase of displacement of about 284 nm (*on average*) during the one-minute hold segment at the maximum load, which is likewise indicative of a significant time-dependent creep-type behavior of electroplated Li. We do observe more variance from sample to sample in the electroplated lithium, which is perhaps due to the presence of SEI and larger surface roughness associated with the electroplated lithium. Overall, our experiments indicate that electroplated Li exhibits similar mechanical properties to bulk Li, particularly in terms of nanoindentation hardness and time-dependent creep behaviors.

Finally, we suggest that our results reported herein have implications in understanding the growth of Li dendrites. The processes of electroplating of lithium and the growth of Li dendrites, while distinct, share similar underlying mechanisms. For instance, both processes occur through reduction of Li ions and deposition of Li during the electrochemical cycling, and both processes are influenced by the current density, the properties of the electrolyte, the state of stress, etc. The key difference is that (uniform) electroplating is a desired and controlled

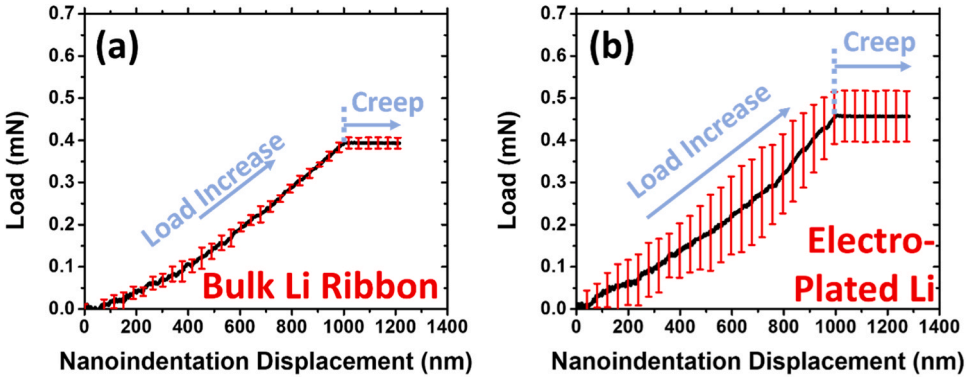


**Fig. 5.** Nanoindentation load-displacement curves of (a) a commercial Li ribbon and (b) electroplated Li. The tests were performed with at constant $\dot{p}/p = 0.05\ s^{-1}$ under mineral oil at room temperature up to a displacement of 1000 nm, followed by holding at the maximum load for one minute. The black line represents the average of six individual tests, and the red bars indicate one standard variation from the average. The individual nanoindentation load-displacement curves can be found in the Supplementary Information Fig. S6.

process, while dendritic growth is an undesirable and potentially dangerous outcome of uncontrolled electrodeposition. It has been hypothesized that in Li-based solid-state batteries, Li dendrites can propagate through a solid electrolyte by filling and widening the small (crack-like) defects within the solid-state electrolyte, oftentimes eventually extending all the way to the cathode[56]. Specifically, mechanical stresses generated by deformation of Li can result in crack-opening of these defects, thereby facilitating further growth of the dendrites (Fig. 6). To address this issue, recent research has focused on designing solid-state electrolytes with improved strength and fracture resistance, aiming to prevent the progression of Li dendrites[33,41].

From a mechanical perspective, providing a better understanding of the mechanics and dynamics of dendritic growth of Li could provide key insight into identifying strategies to prevent their growth, e.g., by identifying appropriate stack pressures, charging conditions, geometries, etc. that are conducive to dendrite-free electrodeposition. It is challenging to identify which of these factors is the most critical in dendrite formation and growth. The interrelationships are highly complex, and various operating conditions, solid electrolyte materials, defects from processing, etc. can contribute to the phenomena [28,56,57]. However, we will point out that local lithium-ion current densities (e.g., around defects/discontinuities) can greatly exceed the globally "applied" current density. As such, we surmise that the effects that we have observed herein, namely that larger current densities induce larger stresses during electrodeposition of lithium, imply that large local stresses can arise from electrodeposition in solid-state systems. Such stresses may induce damage of the solid electrolyte and/or lead to lithium penetration through these defects. Here, we have characterized rate-dependent mechanical behavior associated with electrochemical deposition of Li metal (Figs. 3 and 4), which suggests that the stresses generated during Li dendrite formation (a version of electrodeposition) will depend on the applied current density. Stresses generated during this deposition process (e.g., dendrite formation) govern the forces that are exerted by the deposit (dendrite) on the surrounding environment, i.e., the solid electrolyte. Consequently, crack-driving forces (à la the mechanism indicated in Fig. 6) can be altered by the applied current density.

Additionally, the stack pressure and the current density can affect the electrodeposition behavior of lithium, as well as details of the anode/electrolyte interface in solid-state batteries [42,58]. High current densities often produce non-uniform (dendritic, mossy, porous, etc.) deposition and can alter the plastic flow stress of Li, thereby impacting the overall mechanical stability of the solid-state battery [59,60]. High current densities and increased mechanical stress can lead to unstable Li electrodeposition, as well as cracks/void formation within the material, thereby resulting in irregular growth (*e.g.*, dendrites) and interfacial heterogeneities at the anode/electrolyte interface, and ultimately adversely affecting the performance of solid-state batteries [60]. Likewise, such interfacial heterogeneities result in local stress concentration and induce current crowding (greatly increasing local current densities), which can feed back and exacerbate unstable Li formation penetration within the solid-state electrolyte.

## 4. Conclusions

In this study, we have measured and characterized the mechanical behavior of Li plating at varying current densities. We achieved relatively flat and uniform plating of Li, largely due to the presence of a thin lithiophilic layer of Mg that we deposited prior to electrodeposition of Li. The key result of this study is that we found that the mechanics of Li plating are highly sensitive to the current density. We also performed nanoindentation tests on both bulk and electroplated Li and revealed that their mechanical characteristics are similar. Combining these observations, we surmise that our observed reduction in mechanical stresses during open circuit conditions is due to a combination of mechanics, specifically creeping behavior of Li metal, and chemical side reactions (e.g., dissolution of Li into the electrolyte). Combining these observations, we surmise that our observed reduction in mechanical stresses during open circuit conditions is due to a combination of mechanics, specifically creeping behavior of Li metal, and chemical side reactions (e.g., dissolution of Li into the electrolyte). Beyond having implications in electrodeposition itself, plating of lithium and the growth of lithium dendrites share similar characteristics; as such, our results have further implications for lithium dendrite growth in solid-state electrolytes. For instance, researchers have proposed that "dendrites" in Li-based solid-state batteries can grow by means of lithium filling in (crack-like) defects in the solid-state electrolytes; pressures exerted during this process by Li on the walls of these defects can propagate the defects, causing damage of the solid electrolyte and propagating lithium "dendrites" toward the cathode. Our findings suggest that the crack-driving forces in this scenario (i.e., pressures exerted by Li on the walls of the defects) will strongly depend on the applied current density with larger current densities being likely to induce dendritic growth and ultimately create short circuits in these systems. Overall, this paper has provided fundamental insight into the mechanical characteristics of Li plating during battery cycling, which can aid in designing solid-state batteries and corresponding charging conditions to mitigate mechanical damage during operation.

## CRediT authorship contribution statement

**Jungho Shin:** Writing – original draft, Validation, Software, Formal analysis, Data curation, Conceptualization. **Matt Pharr:** Writing – review & editing, Supervision, Project administration, Funding

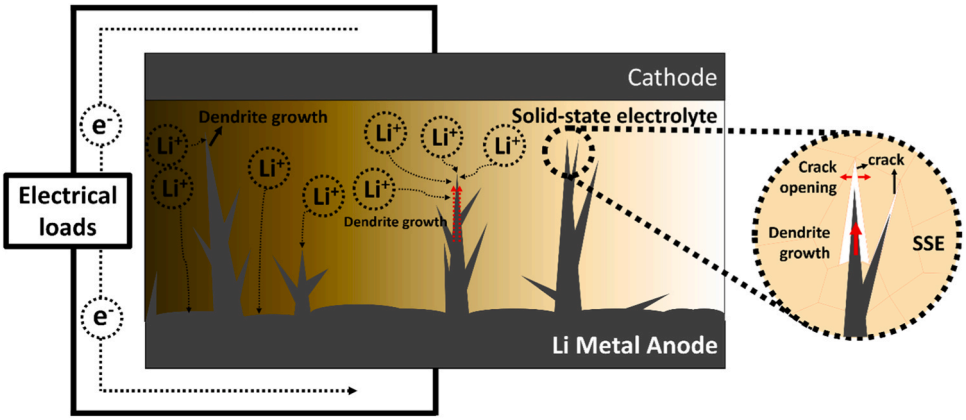


**Fig. 6.** Schematics of Li dendrite penetration into a solid-state electrolyte. The magnified image on the right illustrates a theory of how Li dendrites can propagate micro-cracks inside the solid-state electrolyte. The figure is adapted and modified from Reference #30 [30].

acquisition, Conceptualization.

## Declaration of Competing Interest

The authors declare that they have no known competing financial interests or personal relationships that could have appeared to influence the work reported in this paper.

## Data Availability

Data will be made available on request.

## Acknowledgements

We acknowledge the support of the National Science Foundation, United States under award number DMR-1944674. The authors acknowledge that part of the characterization component of this work was performed in the Texas A & M University Materials Characterization Core Facility (RRID:SCR_022202).

## Appendix A. Supporting information

Supplementary data associated with this article can be found in the online version at doi:10.1016/j.eml.2024.102186.

## References

[1] H. Wu, Y. Cui, Designing nanostructured Si anodes for high energy lithium ion batteries, Nano Today 7 (5) (2012) 414–429.
[2] Z. Zhang, et al., Magnesium anodes with extended cycling stability for lithium-ion batteries, Adv. Funct. Mater. 29 (41) (2019) 1806400.
[3] Y. Hamon, et al., Aluminum negative electrode in lithium ion batteries, J. Power Sources 97 (2001) 185–187.
[4] B. Wang, et al., The dimensionality of Sn anodes in Li-ion batteries, Mater. Today 15 (12) (2012) 544–552.
[5] M. Pharr, Z. Suo, J.J. Vlassak, Variation of stress with charging rate due to strain-rate sensitivity of silicon electrodes of Li-ion batteries, J. Power Sources 270 (2014) 569–575.
[6] Y.S. Choi, et al., A simple technique for measuring the fracture energy of lithiated thin-film silicon electrodes at various lithium concentrations, J. Power Sources 294 (2015) 159–166.
[7] M. Pharr, et al., Kinetics of initial lithiation of crystalline silicon electrodes of lithium-ion batteries, Nano Lett. 12 (9) (2012) 5039–5047.
[8] M. Pharr, et al., Measurements of stress and fracture in germanium electrodes of lithium-ion batteries during electrochemical lithiation and delithiation, J. Power Sources 304 (2016) 164–169.
[9] W. Xu, et al., Lithium metal anodes for rechargeable batteries, Energy Environ. Sci. 7 (2) (2014) 513–537.
[10] B. Liu, J.-G. Zhang, W. Xu, Advancing lithium metal batteries, Joule 2 (5) (2018) 833–845.
[11] X.-B. Cheng, et al., Toward safe lithium metal anode in rechargeable batteries: a review, Chem. Rev. 117 (15) (2017) 10403–10473.
[12] D. Lin, Y. Liu, Y. Cui, Reviving the lithium metal anode for high-energy batteries, Nat. Nanotechnol. 12 (3) (2017) 194–206.
[13] B.S. Vishnugopi, et al., Challenges and opportunities for fast charging of solid-state lithium metal batteries, ACS Energy Lett. 6 (10) (2021) 3734–3749.
[14] F. Wu, et al., Perspectives for restraining harsh lithium dendrite growth: Towards robust lithium metal anodes, Energy Storage Mater. 15 (2018) 148–170.
[15] J. Pu, et al., Interlayer lithium plating in Au nanoparticles pillared reduced graphene oxide for lithium metal anodes, Adv. Funct. Mater. 28 (41) (2018) 1804133.
[16] L. Liu, et al., Uniform lithium nucleation/growth induced by lightweight nitrogen-doped graphitic carbon foams for high-performance lithium metal anodes, Adv. Mater. 30 (10) (2018) 1706216.
[17] J.H. Cho, et al., Stress evolution in lithium metal electrodes, Energy Storage Mater. 24 (2020) 281–290.
[18] K.N. Wood, M. Noked, N.P. Dasgupta, Lithium metal anodes: toward an improved understanding of coupled morphological, electrochemical, and mechanical behavior, ACS Energy Lett. 2 (3) (2017) 664–672.
[19] Y. Liu, et al., Lithium-coated polymeric matrix as a minimum volume-change and dendrite-free lithium metal anode, Nat. Commun. 7 (1) (2016) 1–9.
[20] Y. Zhang, et al., High-capacity, low-tortuosity, and channel-guided lithium metal anode, Proc. Natl. Acad. Sci. 114 (14) (2017) 3584–3589.
[21] J.H. Cho, et al., An investigation of chemo-mechanical phenomena and Li metal penetration in all-solid-state lithium metal batteries using in situ optical curvature measurements, Adv. Energy Mater. (2022) 2200369.
[22] K.-H. Chen, et al., Dead lithium: mass transport effects on voltage, capacity, and failure of lithium metal anodes, J. Mater. Chem. A 5 (23) (2017) 11671–11681.
[23] D. Tewari, P.P. Mukherjee, Mechanistic understanding of electrochemical plating and stripping of metal electrodes, J. Mater. Chem. A 7 (9) (2019) 4668–4688.
[24] A.J. Sanchez, et al., Plan-view operando video microscopy of Li metal anodes: identifying the coupled relationships among nucleation, morphology, and reversibility, ACS Energy Lett. 5 (3) (2020) 994–1004.
[25] M.L. Meyerson, et al., The effect of local lithium surface chemistry and topography on solid electrolyte interphase composition and dendrite nucleation, J. Mater. Chem. A 7 (24) (2019) 14882–14894.
[26] G. Bieker, M. Winter, P. Bieker, Electrochemical in situ investigations of SEI and dendrite formation on the lithium metal anode, Phys. Chem. Chem. Phys. 17 (14) (2015) 8670–8679.
[27] R. Zhang, et al., Lithiophilic sites in doped graphene guide uniform lithium nucleation for dendrite-free lithium metal anodes, Angew. Chem. 129 (27) (2017) 7872–7876.
[28] C.D. Fincher, et al., Controlling dendrite propagation in solid-state batteries with engineered stress, Joule 6 (12) (2022) 2794–2809.
[29] G. McConohy, et al., Mechanical regulation of lithium intrusion probability in garnet solid electrolytes, Nat. Energy (2023) 1–10.
[30] L. Porz, et al., Mechanism of lithium metal penetration through inorganic solid electrolytes, Adv. Energy Mater. 7 (20) (2017) 1701003.
[31] C. Yuan, B.W. Sheldon, J. Xu, Heterogeneous reinforcements to mitigate Li penetration through solid electrolytes in all-solid-state batteries, Adv. Energy Mater. 12 (39) (2022) 2201804.
[32] L. Yu, J. Wang, Z.J. Xu, A perspective on the behavior of lithium anodes under a magnetic field, Small Struct. 2 (1) (2021) 2000043.
[33] C.E. Athanasiou, et al., High-toughness inorganic solid electrolytes via the use of reduced graphene oxide, Matter 3 (1) (2020) 212–229.
[34] Y.-G. Lee, et al., High-energy long-cycling all-solid-state lithium metal batteries enabled by silver–carbon composite anodes, Nat. Energy 5 (4) (2020) 299–308.
[35] W.S. LePage, et al., Lithium mechanics: roles of strain rate and temperature and implications for lithium metal batteries, J. Electrochem. Soc. 166 (2) (2019) A89–A97.
[36] C.D. Fincher, et al., Mechanical properties of metallic lithium: from nano to bulk scales, Acta Mater. 186 (2020) 215–222.
[37] A. Masias, et al., Elastic, plastic, and creep mechanical properties of lithium metal, J. Mater. Sci. 54 (3) (2019) 2585–2600.
[38] M. Pharr, Z. Suo, J.J. Vlassak, Measurements of the fracture energy of lithiated silicon electrodes of Li-ion batteries, Nano Lett. 13 (11) (2013) 5570–5577.
[39] W.C. Oliver, G.M. Pharr, An improved technique for determining hardness and elastic modulus using load and displacement sensing indentation experiments, J. Mater. Res. 7 (6) (1992) 1564–1583.
[40] O. Crowther, A.C. West, Effect of electrolyte composition on lithium dendrite growth, J. Electrochem. Soc. 155 (11) (2008) A806.
[41] C.E. Athanasiou, et al., Operando measurements of dendrite-induced stresses in ceramic electrolytes using photoelasticity, Matter 7 (1) (2024) 95–106.
[42] C. Fang, et al., Pressure-tailored lithium deposition and dissolution in lithium metal batteries, Nat. Energy 6 (10) (2021) 987–994.
[43] Z. Huang, et al., Seeding lithium seeds towards uniform lithium deposition for stable lithium metal anodes, Nano Energy 61 (2019) 47–53.
[44] R. Pathak, Y. Zhou, Q. Qiao, Recent advances in lithiophilic porous framework toward dendrite-free lithium metal anode, Appl. Sci. 10 (12) (2020) 4185.
[45] S.-H. Wang, et al., Tuning wettability of molten lithium via a chemical strategy for lithium metal anodes, Nat. Commun. 10 (1) (2019) 4930.
[46] S. Kanamori, et al., Lithium metal deposition/dissolution under uniaxial pressure with high-rigidity layered polyethylene separator, RSC Adv. 10 (30) (2020) 17805–17815.
[47] Z. Guo, et al., Lithiophilic Co/Co 4 N nanoparticles embedded in hollow N-doped carbon nanocubes stabilizing lithium metal anodes for Li–air batteries, J. Mater. Chem. A 6 (44) (2018) 22096–22105.
[48] K. Park, J.B. Goodenough, Dendrite-suppressed lithium plating from a liquid electrolyte via wetting of Li3N, Adv. Energy Mater. 7 (19) (2017) 1700732.
[49] G.G. Stoney, The tension of metallic films deposited by electrolysis, Proc. R. Soc. Lond. Ser. A, Contain. Pap. A Math. Phys. Character 82 (553) (1909) 172–175.
[50] S. Ding, et al., Compressive creep deformation of lithium foil at varied cell conditions, J. Power Sources 488 (2021) 229404.
[51] G. Regazzoni, U. Kocks, P.S. Follansbee, Dislocation kinetics at high strain rates, Acta Metall. 35 (12) (1987) 2865–2875.
[52] L.B. Freund, S. Suresh, Thin film materials: stress, defect formation and surface evolution, Cambridge university press, 2004.
[53] A.L. Shull, F. Spaepen, Measurements of stress during vapor deposition of copper and silver thin films and multilayers, J. Appl. Phys. 80 (11) (1996) 6243–6256.
[54] J. Floro, et al., The dynamic competition between stress generation and relaxation mechanisms during coalescence of Volmer–Weber thin films, J. Appl. Phys. 89 (9) (2001) 4886–4897.
[55] P. Sayavong, et al., Dissolution of the solid electrolyte interphase and its effects on lithium metal anode cyclability, J. Am. Chem. Soc. 145 (22) (2023) 12342–12350.
[56] Z. Ning, et al., Dendrite initiation and propagation in lithium metal solid-state batteries, Nature 618 (7964) (2023) 287–293.
[57] M.J. Wang, R. Choudhury, J. Sakamoto, Characterizing the Li-solid-electrolyte interface dynamics as a function of stack pressure and current density, Joule 3 (9) (2019) 2165–2178.

[58] D. Chatterjee, et al., Electrodeposition stability landscape for solid–solid interfaces, Adv. Sci. (2023) 2307455.
[59] S. Sarkar, V. Thangadurai, Critical current densities for high-performance all-solid-state Li-metal batteries: fundamentals, mechanisms, interfaces, materials, and applications, ACS Energy Lett. 7 (4) (2022) 1492–1527.
[60] Y. Tang, et al., Electro-chemo-mechanics of lithium in solid state lithium metal batteries, Energy Environ. Sci. 14 (2) (2021) 602–642.